JOURNAL OF SPACECRAFT AND ROCKETS
Vol. 44, No. 1, January–February 2007

Experimental Study on Aerodynamic Characteristics of Telescopic Aerospikes with Multiple Disks

Hiroaki Kobayashi*
Japan Aerospace Exploration Agency, Chofu, Tokyo 182-8522, Japan
Yusuke Maru†
University of Tokyo, Bunkyo, Tokyo 113-8656, Japan
and
Katsuyoshi Fukiba‡
Japan Aerospace Exploration Agency, Sagamihara, Kanagawa 229-8510, Japan

DOI: 10.2514/1.25250

In this paper, experimental studies on telescopic aerospikes with multiple disks are reported. The telescopic aerospike is useful as an aerodynamic control device; however, changing its length causes a buzz phenomenon, which many researchers have reported. The occurrence of buzzing might be critical to the vehicle because it brings about severe pressure oscillations on the surface. Disks on the shaft produce stable recirculation regions by dividing the single separation flow into several conical cavity flows. Therefore, the telescopic aerospikes with stabilizer disks are useful without being any length constraints. Aerodynamic characteristics of the telescopic aerospikes were investigated using wind tunnel tests. Transition of recirculation/reattachment flow modes of a plain spike causes a large change in the drag coefficient. Because of this hysteresis phenomenon, the plain spike is unsuitable for fine aerodynamic control devices. Adding stabilizer disks is effective for the improved control of aerospikes.

Nomenclature

C_D	=	drag coefficient
C_L	=	lift coefficient
$C_{L\alpha}$	=	lift coefficient line slope
D	=	base cylinder diameter
L	=	aerospike length
L/D	=	aerospike length to base cylinder diameter ratio
M	=	Mach number
N_d	=	number of stabilizer disks
X_{cp}	=	distance measuring from spike tip to position of center of pressure, which is normalized by total length of model ($10.3D$)
α	=	angle of attack
ΔC_D	=	change in C_D in translating spike
$\Delta(L/D)$	=	change in L/D in spike translation
δ	=	half cone angle

Introduction

AEROSPIKES are aerodynamic devices for rockets, missiles, and reentry vehicles. Separated flow that is formed around the aerospike reduces the wave drag and heat-transfer rates on the nose surface of vehicles in supersonic and hypersonic flight conditions.

Several application cases of aerospikes exist already. The M-3S-II rocket, the Japanese solid booster, has fixed aerospikes at the top of its two strap-on boosters to reduce atmospheric drag during its ascent. Tridents I and II are spike-nosed submarine-launched ballistic missiles. After the Trident missile is fired from a submarine, the first stage motor ignites and the aerospike extends. The missile's range is increased by the aerospike, which reduces drag by 50% [1]. Aerospikes are not only used for drag reduction. The high explosive antitank (HEAT) M830, which is fired from the M1A1 tank, is a spike-nosed projectile [2,3]. The M830 projectile's spike serves as an impact sensor. In 2004, Henne et al. [4] proposed supersonic aircraft with spikes for controlling and reducing sonic booms. By extending the spike forward from the leading edge of the fuselage or rearward from the trailing edge of the fuselage, the sonic boom amplitude at ground level is reduced.

The separation flow around the aerospike is essentially unstable. Therefore, many researchers have reported on its aerodynamic characteristics. In the early 1950s, Robins [5] conducted an investigation to determine the effect of several seeker-nose configurations (cone spike, plain spike, slotted cone, spherical, conical, and parabolic) on the static longitudinal stability, the canard control characteristics, and lift and drag of a canard-type ramjet missile. Kubota et al. [6] also studied the feasibility of using spikes as drag and heat-transfer rate reducing devices on blunt bodies at hypersonic speeds. Mikhail [7,8] investigated dual flow modes of spike-nosed projectile configurations, pointing out that flow oscillation between the high-drag mode and the low-drag mode causes a buzzing phenomenon. In later studies, he conducted numerical simulations of the spike-nosed projectile with a tripping ring at the spike tip for preventing a high-drag mode. Feszty et al. [9,10] reported the driving mechanism of two distinct spike-induced unsteady flow modes: oscillation and pulsation. The oscillation flow mode is characterized by the foreshock shape change between a convex shape and a concave one, whereas the shock system changes dramatically in the pulsation flow mode. The oscillation mode is typical of longer spike lengths ($L/D = 1.5$–2.5) and the pulsation mode of shorter ones ($L/D = 0.2$–1.5). Maurer et al. [11] observed a sudden increase in the drag of a very long spiked body because the tip-disk wake reattaches onto the spike shaft. Once the flow attaches onto the spike shaft, it remains attached until it separates again near the nose because of the adverse pressure gradient of the forward facing step of the nose. Srinivasan et al. [12] reported the effect of spike length and external burning on the drag of the hemisphere nose cylinder. They showed that hydrogen injection and burning can eliminate reattachment of the shock wave, thereby reducing the drag

Received 18 May 2006; revision received 9 August 2006; accepted for publication 13 August 2006.

*Research Associate, Institute of Aerospace Technology, Aeroengine Technology Center, 7-44-1 Jindaiji-higashimachi. Member AIAA.

†JSPS Research Fellow, Department of Aeronautics and Astronautics, 7-3-1 Hongo. Member AIAA.

‡Aerospace Project Research Associate, Institute of Space and Astronautical Science, Department of Space Transportation Engineering, 3-1-1 Yoshinodai.

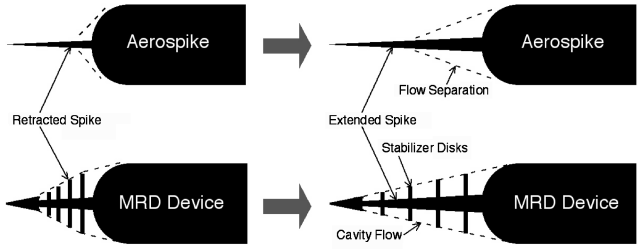

Fig. 1 Schematic view of the flow field around the aerospike.

of spiked missiles. Menezes et al. [13,14] evaluated the effect of retractable aerospikes (flat disk spike, hemispherical spike, flat spike, and sharp spike) as drag reducing devices on a large-angle blunt cone. Results indicate ca. 40–55% drag reduction for the blunt cone using flat and hemispherical aerodisks at a lower angle of attack (up to ca. 5 deg).

The telescopic aerospike is useful as an aerodynamic control device; however, changing its length causes a buzz phenomenon, which many researchers have reported. The occurrence of buzzing might be critical to the vehicle because it brings about severe pressure oscillations on the surface. Reding [15] pointed out that the aerospike adversely affects aerodynamic dumping to certain critical free-free bending modes. A detailed aeroelastic analysis should be conducted to ensure the structural integrity of the vehicle and aerospike.

Figure 1 shows our newly invented aerospike configuration with stabilizer disks, which is designated the multiple-row-disk (MRD) device, as well as the conventional plain aerospike. The disks on the shaft produce a stable recirculation region by dividing the single separation flow into several conical cavity flows. Buzzing phenomena are not observed in deep cavity flow. Therefore, telescopic aerospikes with stabilizer disks are useful without being any length constraints. Shvets et al. [16] conducted an experimental study on the axisymmetric cavity flow of cone-cylinder body. Nestler [17] reported the effect of a rectangular cavity on 9 deg cone surface on aerodynamic forces. Viswanathan et al. [18] conducted detached eddy simulation of the flow around the cone-cylinder body with an axisymmetric cavity. The preceding studies show that axisymmetric cavity flow is similar to the cavity flow on a flat plate when the angle of attack is 0 deg. Margason et al. [19] reported the feasibility of use of multiple cavities as an airfoil high-lift device. Experimental and computational investigations have shown that multiple open cavities in either zero or adverse pressure gradients produce only small changes in boundary layer characteristics. Results also showed that a small backward facing step created larger, adverse changes to the boundary layer than those produced by the cavities.

We investigated multiple-cavity flow on the conical surface [20,21]. We found that an increased number of disks put in the cavity for a stabilizing shear layer is effective. Benefits of increasing the disk number are the following:

1) Decreasing boundary layer thickness at the downstream of cavities.

2) Suppression of pressure oscillation in and out of cavities and structural vibration.

This paper reports experimental studies on telescopic aerospikes with multiple disks. First, effects of axisymmetric cavities on the aerodynamic characteristics of conical nose were investigated. Second, a parametric study of steady state aerodynamic characteristics of the aerospike were performed, including the effects of spike length and disk number. Third, verification tests of telescopic aerospikes were conducted to elucidate its control of aerodynamic characteristics. Changes of aerodynamic forces in extending or retracting spikes were measured.

Aerodynamics of Axisymmetric Cavities on the Conical Nose

Experimental Setup

The experimental investigation of effects of axisymmetric cavities on aerodynamic characteristics of conical nose were performed in 0.6×0.6 m supersonic and transonic wind tunnels at the Institute of Space and Astronautical Science (ISAS), Japan Aerospace Exploration Agency (JAXA). Part a) of Table 1 shows those test conditions. The Mach number was 0.9–3.0 and the angle of attack was −4–14 deg. Figure 2 shows an image and a definition of dimensions of the wind tunnel test model with a 40-mm-diameter cylindrical fuselage and 8 deg half-angle cone. A six-component strain-gauge balance is housed in the model to measure lift, drag, and static stability for four nose shapes. An accuracy of the balance is ±0.5% of its full range. The measurement ranges of the balance are also presented in Table 2. Table 3 shows geometric characteristics of tested models. A straight cone without a cavity was tested for reference, which has an apex angle of 16 deg. "Short cavity" has a single 10.7-mm-long cavity. The cavity length to depth ratio is approximately 1. "Long cavity" has a single 28.4-mm-long cavity, which is designed to evaluate the effect of cavity length through comparison with short cavity. The cavity length to depth ratio is approximately 3. "Three cavity" has three deep and short cavities. The objective of this model is to evaluate the effect of cavity number on the aerodynamic force. The total length of cavities of three cavity is equal to that of long cavity.

Results

Figure 3 shows the drag coefficient variation according to the angle of attack for four nose types. The reference area of the drag coefficient is the section area of the 40-mm-diameter cylinder. Predicted values with empirical expressions of the conical nose drag, Eq. (1), are also plotted on a graph showing $C_{L\alpha}$ of the measured value was used.

$$C_D = (0.0016 + 0.002/M^2)\delta^{1.7} + C_{L\alpha}\alpha^2 \tag{1}$$

Table 1 Wind tunnel test conditions

Mach number	Stagnation temperature, K	Stagnation pressure, MPa	Dynamic pressure, kPa	Reynolds number, 10^7 m^{-1}
		a) ISAS/JAXA 0.6×0.6 m *supersonic/transonic wind tunnel*		
1.1	288	0.147	58.3	2.31
1.5	288	0.196	84.1	3.00
3.0	288	0.441	75.6	3.47
		b) IAT/JAXA 1.0×1.0 m *supersonic wind tunnel*		
1.5	288	0.160	68.6	2.45
2.0	288	0.220	78.7	2.84
2.5	288	0.320	81.9	3.26
3.0	288	0.510	87.5	4.01
3.5	288	0.780	87.7	4.76
		c) IAT/JAXA Φ0.5 m *hypersonic wind tunnel*		
5.1	630	1.00	30.6	0.845

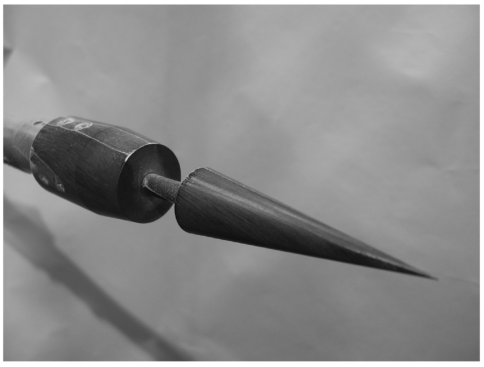

a) Image, Long cavity

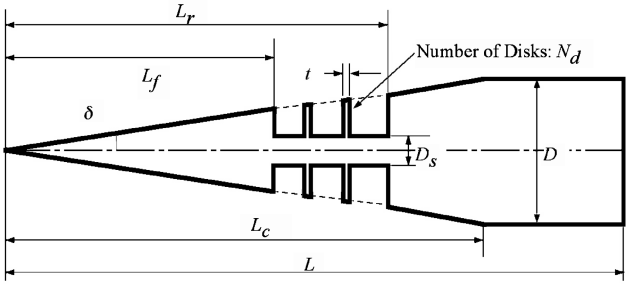

b) Definition of geometric parameter dimensions

Fig. 2 Wind tunnel test model.

The short cavity nose can match the straight cone in terms of drag coefficient, whereas the long cavity produces more drag. The drag coefficient increases with the total length of cavities on the nose surface. High pressure on the rear face of the shallow cavity causes additional drag on the nose. Figure 4 shows oil flow visualizations at 2 and 10 deg angles of attack. Stable circulating flows are visible in the cavity at a 2 deg angle of attack. The separation line on the shaft indicates a two-vortex flow structure, which is typical of a deep cavity. In the cavity at a 10 deg angle of attack, the two-vortex flow structure is maintained windward, whereas a more complicated flow pattern is visible leeward because of secondary flow from windward to leeward. The pressure balance along the cavity floor is lost because of this secondary flow, thereby increasing drag. Another important observation arises from a comparison between the long cavity and the three cavity. Drag coefficient of the three cavity is smaller than that of the long cavity at every angle of attack. This result indicates that for the same total length of cavities, an increased number of stabilizer disks is effective for reduction of both zero-lift drag and induced drag.

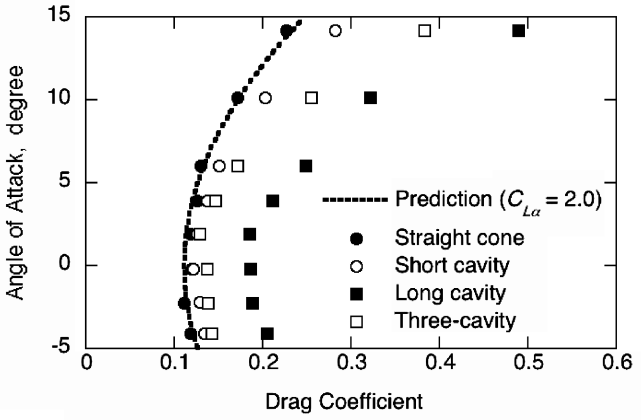

a) Mach 1.1

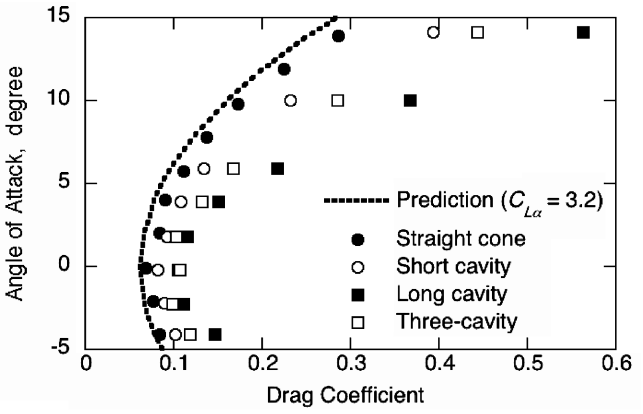

b) Mach 3.0

Fig. 3 Variation of the drag coefficient with the angle of attack: a) Mach 1.1; b) Mach 3.0.

Aerodynamic Characteristics of Fixed Length Aerospikes

Experimental Setup

Wind tunnel experiments on fixed geometry aerospikes were conducted to evaluate the effects of geometric parameters, including spike length and number of disks, on aerodynamic characteristics in a 1.0×1.0 m supersonic wind tunnel and a $\Phi 0.5$ m hypersonic wind tunnel at the Institute of Aerospace Technology (IAT), JAXA. The test conditions are summarized in parts b) and c) of Table 1. The Mach number ranged from 1.5–4.0 at supersonic wind tunnel, and was 5.1 at hypersonic wind tunnel. The angle of attack ranged from

Table 2 Measurement ranges of force balance

	ISAS supersonic/transonic WT	IAT supersonic WT	IAT hypersonic WT
Axial force, N	196.0	800.0	147.0
Normal force, N	980.0	5000.0	686.0
Pitching moment, N · m	39.2	300.0	24.5

Table 3 Geometric characteristics of the test model

Model	Straight cone	Short cavity	Long cavity	Three cavity
D, mm	40.0	40.0	40.0	40.0
δ, deg	8.0	8.0	8.0	8.0
L, mm	182.3	182.3	182.3	182.3
L_c, mm	142.3	142.3	142.3	142.3
N_d	——	——	——	2
t, mm	——	——	——	2
L_f, mm	——	106.2	88.7	84.7
L_r, mm	——	116.8	116.8	116.8
D_s, mm	——	7.3	8.6	8.6

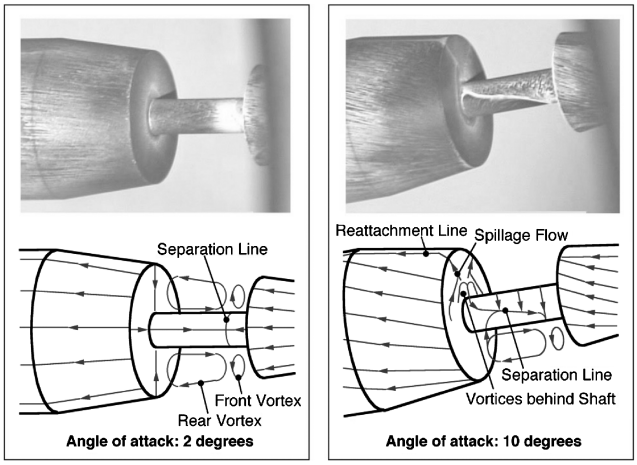

Fig. 4 Oil flow visualization of long cavity, Mach 1.5.

−6–14 deg. Aerodynamic forces on five types of aerospikes, as shown in Table 4 and Fig. 5, were measured using a six-component stress wave force balance. An accuracy of the balances is ±0.5% of its full range. The measurement ranges of the balances are also presented in Table 2. "Cone" without a cavity has 24 deg-apex angle. The cone is divided into two parts: a tip cone of 14 mm base diameter and an adjacent truncated cone. The truncated cone is replaceable with longer and shorter ones by 0.5D. "Cone M" denotes the straight cone of reference length, whereas "cone S" and "cone L," respectively, denote the short cone configuration and the long one. "Aerospike" is a 14-mm-diameter plain spike, whereas "single disk," "three disk," and "six disk," respectively, have a single disk, three disks, and six disks on the shaft. The reference spike length of these models is 2.15D. The spike length can be 1.65D for the short spike configuration and 2.65D for the long one.

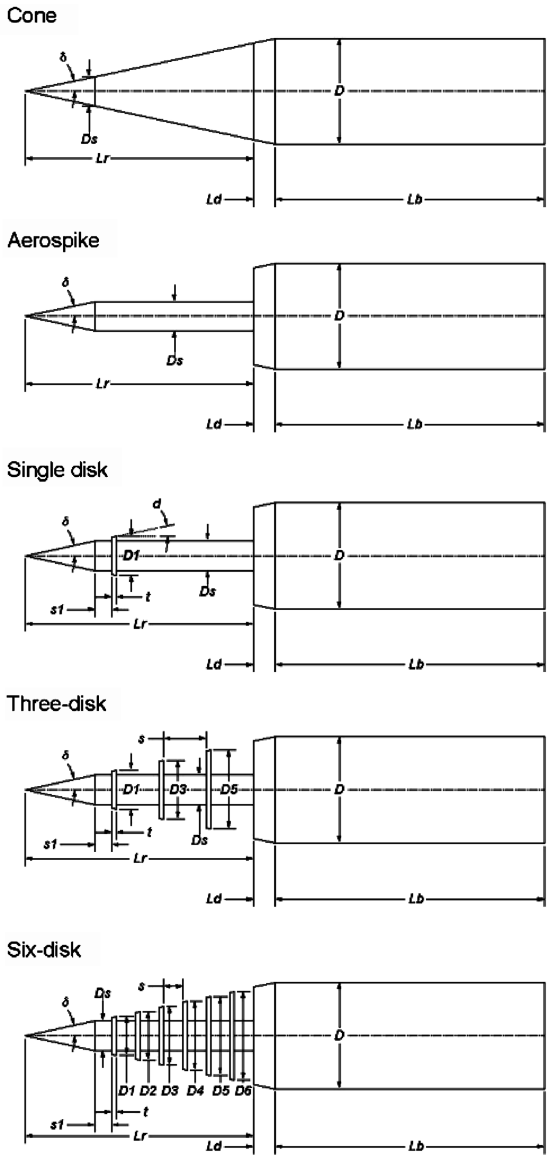

Fig. 5 Schematic view of the test model.

Results

Figure 6 shows flow fields around aerospike M and six disk M at Mach 2, high angle of attack (14 deg). A distinctively strong bow shock is observed on the windward side of the aerospike M, although a large recirculation flow region is formed on the leeward side. This image shows that the plain aerospike cannot maintain a separation flow at a high angle of attack. In contrast, the flow field around the six disk M does not include a strong bow shock, but rather weak oblique shocks from each disk because of the flow stability in deep cavities between adjacent disks.

Figure 7 depicts a comparison of drag coefficient variation according to the angle of attack at Mach 2 conditions to evaluate the effect of geometric parameters, aerospike length and the number of disks. As for the cone, the drag coefficient of the long one (cone L) is lower than that of the short one (cone S) at every angle of attack. This result shows that the cone, which changes its cone angle, has ideal performance as an axial force control device; however, advanced

Table 4 Geometric characteristics of aerospikes

Model	Cone/aerospike			Single disk			Three disk			Six disk		
Length	M	S	L	M	S	L	M	S	L	M	S	L
L_r, mm	107.6	82.6	132.6	107.6	82.6	132.6	107.6	82.6	132.6	107.6	82.6	132.6
s, mm		——			——		20.2	11.9	28.6	9.1	4.9	13.3
$s1$, mm		——			8.0			8.0			8.0	
t, mm		——			2.0			2.0			2.0	
N_d		——			1			3			6	
δ, degree		12.0			12.0			12.0			12.0	
L_b, mm		397.0			397.0			397.0			397.0	
L_d, mm		10.0			10.0			10.0			10.0	
D, mm		50.0			50.0			50.0			50.0	
D_s, mm		14.0			14.0			14.0			14.0	
$D1$, mm		——			18.3			18.3			18.3	
$D2$, mm		——			——			——			23.0	
$D3$, mm		——			——			27.7			27.7	
$D4$, mm		——			——			——			32.4	
$D5$, mm		——			——			37.2			37.2	
$D6$, mm		——			——			——			41.9	

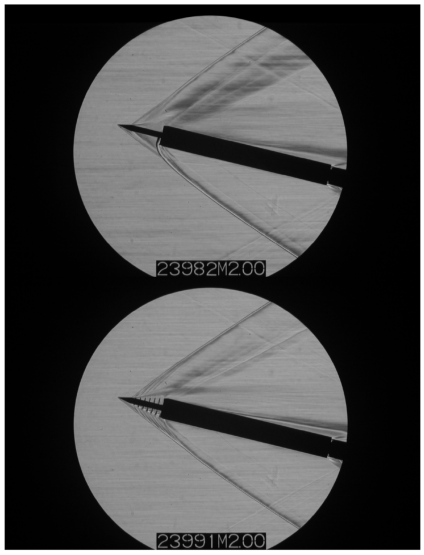

Fig. 6 Schlieren photographs showing the flow field around aerospike M (upper) and six disk M (lower), Mach 2.0, angle of attack = 14 deg.

elastic materials should be developed to actualize this type of aerodynamic device. Figure 7b shows that the telescopic aerospike can change its axial force only at a very low angle of attack. Still worse, the drag coefficient of aerospike L, with the longest spike, is larger than that of the aerospike M. A translating plane spike cannot control aerodynamic forces because it causes subtle changes in the flow structure of the recirculation region. The aerodynamic axial force control can be improved by increasing the number of stabilizer

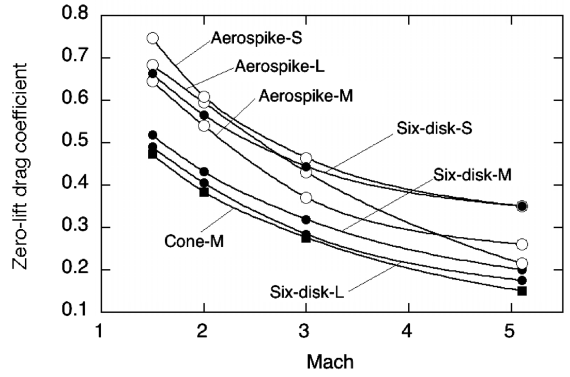

Fig. 8 Variation of the zero-lift drag coefficient with Mach number.

disks. The six disk can change its drag coefficient by retracting or extending the spike as the cone in the angle of attack range of −4 to 4 deg. Effects of stabilizer disks are visible in Fig. 8, which shows the variation of the zero-lift drag coefficient with Mach numbers. However, the drag coefficient of an aerospike with disks increases by extending the spike at a high angle of attack. The lift coefficient is almost independent of the spike length. Therefore, the drag increase is not the result of the induced drag of the extended spike. Deterioration of aerodynamic controllability at a high angle of attack is presumably caused by shallow cavity flows, which are formed between disks on the extended aerospike, resulting in increased unbalanced pressure on disk surfaces.

Figure 9 shows a sudden change in the drag coefficient of the single disk L at a 4 deg angle of attack. This phenomenon was observed independently of the angle of attack sweep rate. Flow

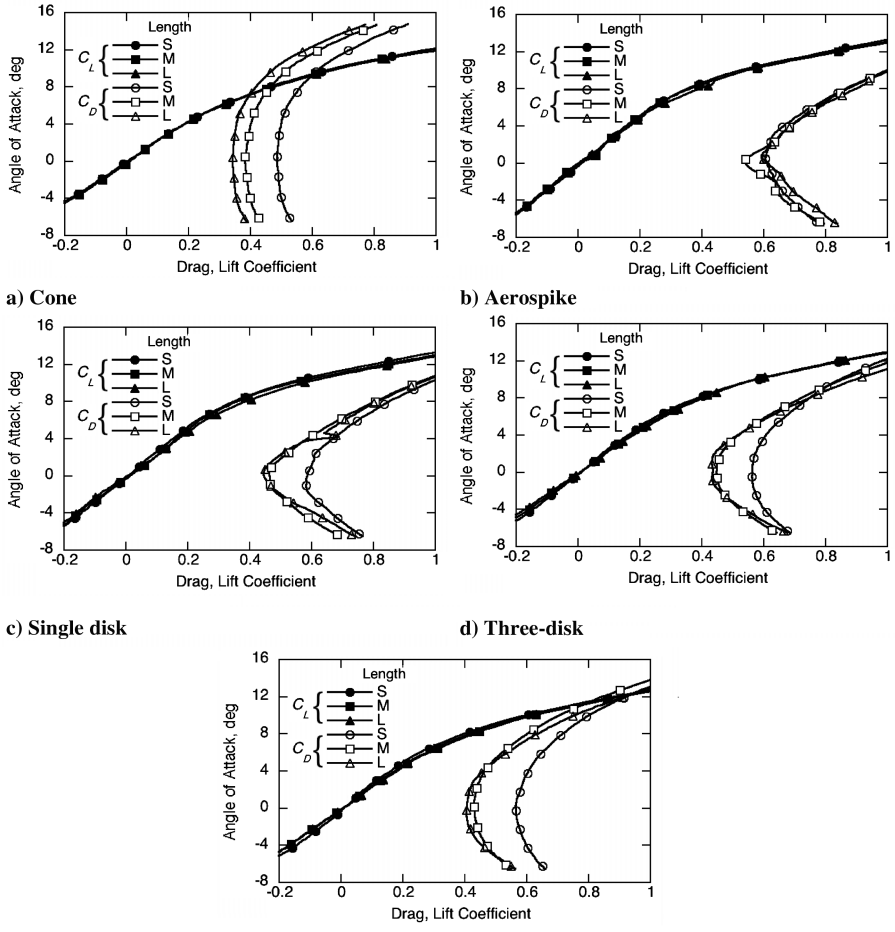

Fig. 7 Variation of drag coefficient and lift coefficient with angle of attach at Mach 2.0.

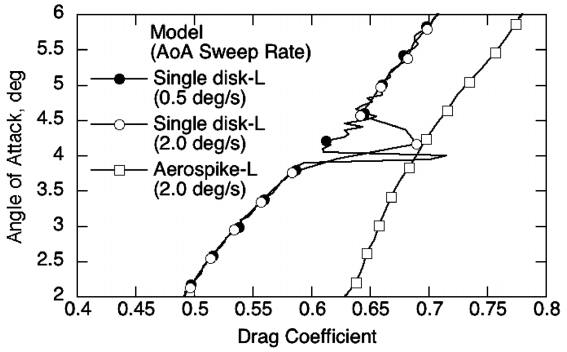

Fig. 9 Effect of separation flow reattachment on drag coefficient of single disk L.

reattachment on the middle surface of the spike was observed in Schlieren photographs only for the 4 deg angle of attack. This flow mode change is similar to phenomena reported by Maurer et al. [11]. The increased drag coefficient of the single disk L matches that of the aerospike L. At a higher angle of attack than 4 deg, the flow separates again and drag decreases suddenly.

Figure 10 presents a comparison of the center of pressure (Xcp) of the cone M, the aerospike M, and the six disk M. Xcp, which is the distance between the spike tip and the center of pressure, is normalized by the total length of models ($10.3D$). The Xcp of the aerospike M is longer than that of the cone M by 30%, which means that the aerospike M is superior to the cone M in static longitudinal stability. The Xcp variation of the six disk M with the Mach number more closely resembles that of the aerospike M than the cone M because the spike configurations of the aerospike M and the six disk M mainly produce axial force, not lateral force. Therefore, the aerospike with the stabilizer disks improves both drag characteristics and static stability. Using the aerospike with the stabilizer disks, arbitrary aerodynamic control can be achieved without degrading aerodynamic characteristics, as do other aerospike configurations.

Unsteady Aerodynamics of Telescopic Aerospikes

Experimental Setup

Aerodynamic characteristics of telescopic aerospikes were investigated using wind tunnel tests. Figure 11 shows a schematic diagram of the aerospike test models. A spike shaft with a 24 deg tip cone is installed on the front face of the 50-mm-diameter (D) cylindrical body. An aerospike with three disks is shown in Fig. 12; it has the same configuration as the three disk described in Table 4 and Fig. 5. Spike length (L) can be changed pneumatically by 50 mm ($=1.0D$) to measure variations of aerodynamic forces according to the spike length. The spike extends forward by supplying pressured air into the cylindrical body. The spike's transit time from the shortest configuration to the longest was 3 s. The spike retracts quickly backward with an inner spring when the air in the body is vented. Three springs were installed between disks to synchronize the displacement of each disk with the translating spike. The spike length was measured by reading off on video images. Uncertainties of the measured length are $\pm 0.02D$. Experiments were conducted using the IAT/JAXA 1.0 m $\times$ 1.0 m supersonic wind tunnel. The Mach number ranged from 1.5–3.0 and the angle of attack is 0 and 4 deg.

Results

Figure 13 shows Schlieren photographs of the flow field around telescopic aerospikes at Mach 1.5. Pulsation mode, which was investigated by Feszty et al. [9,10], was observed around the plain short spike at $\alpha = 0$ deg, Fig. 13b. The dynamic change of shock system in the pulsation mode is shown in Fig. 14. Stable separation flow without a buzz phenomenon was formed around the extended spike, Fig. 13a. Flow around the plain short spike at $a = 4$ deg, Fig. 13d, was as oscillatory as Fig. 13b, whereas reattachment flow mode was observed around extended plain spike, Fig. 13c. Separation flow behind the tip cone reattaches onto the leading edge

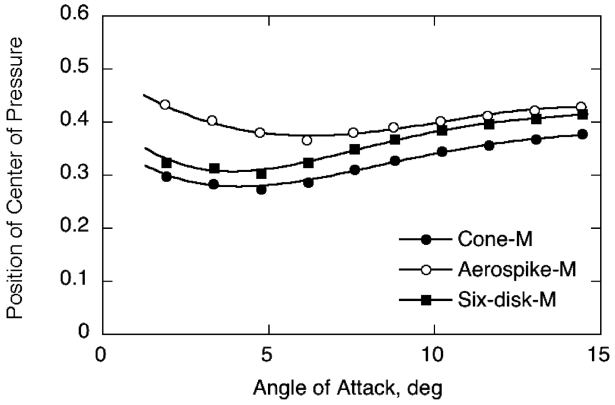

a) Mach 1.5

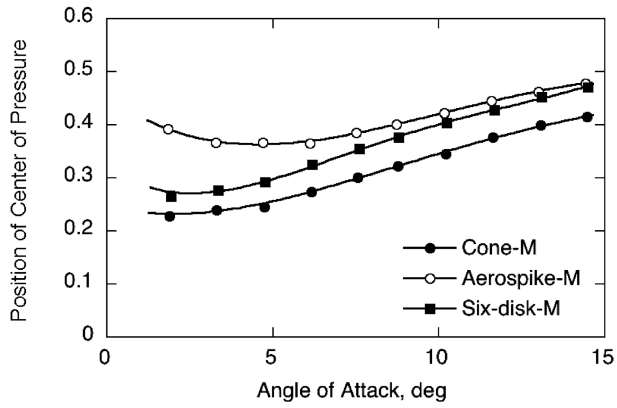

b) Mach 2.0

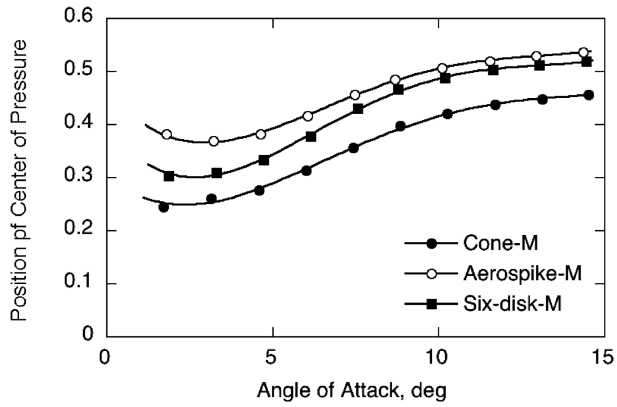

c) Mach 3.0

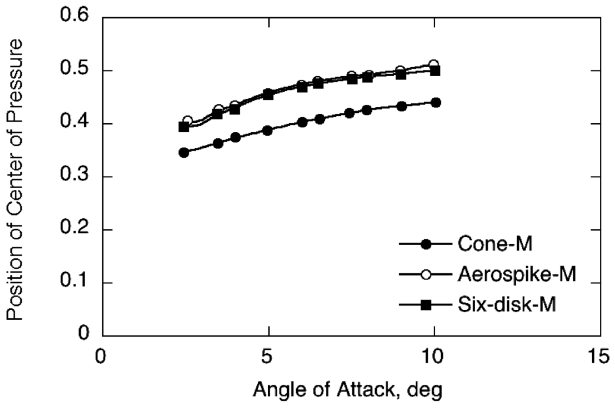

d) Mach 5.1

Fig. 10 Variation of position of center of pressure with the angle of attack.

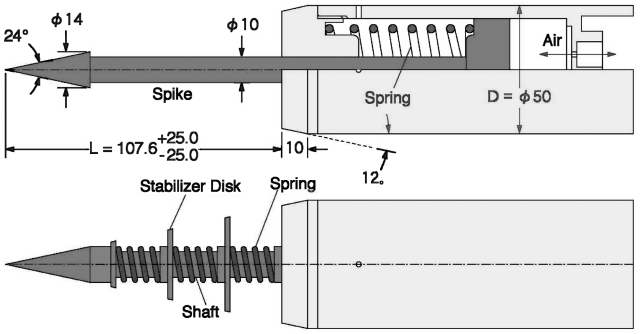

Fig. 11 Schematic diagram of the telescopic aerospikes.

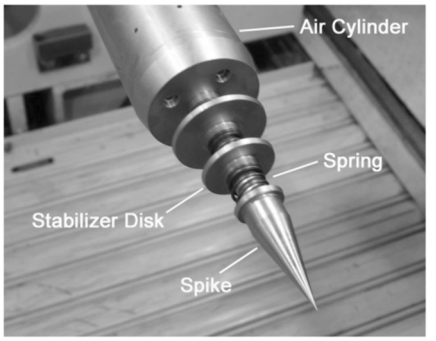

Fig. 12 Photograph of the test model.

of the body cylinder when the spike shaft is short. The reattachment point jumps onto the spike shaft while extending the spike, thereby contracting the recirculation flow region.

Figure 15 shows different flow modes around the extended plain spike at $\alpha = 0$. The reattachment flow mode shown in Fig. 15a was observed when the angle of attack of the extended plain aerospike changes from 4 to 0 deg, whereas separation flow mode continues unless the angle of attack is changed, as shown in Fig. 15b. The transition of reattachment/separation flow modes is therefore not only dependent on free stream conditions and geometric configurations. It is also affected by adjacent states, that is, hysteresis phenomenon. Figure 16 shows the drag coefficient variation (C_D) with spike length to the base diameter ratio (L/D) for the plain aerospike without a disk. The C_D decreases with increasing L/D(1.8–2.2) at $\alpha = 0$ deg, whereas C_D of the plain aerospike with 4 deg angle of attack suddenly increases at $L/D = 2.2$ by 0.17 attributable to the flow mode transition from separation to reattachment. The C_D at $\alpha = 4$ deg was independent of L/D between $L/D = 2.2$–2.7 as that at $\alpha = 0$ deg. The C_D variations at $\alpha = 0$ deg and at $a = 4$ deg remained nearly constant between $L/D = 2.2$–2.7. The C_D of reattachment flow mode at $\alpha = 0$ deg, $L/D = 2.7$ [Fig. 15a] is higher than that of separation flow mode [Fig. 15b] by 0.15. Figure 17 shows the variation of C_D with L/D for the aerospike with three disks. Adding stabilizer disks is effective for improved controllability of C_D between $L/D = 2.0$–2.7. Pulsation mode and hysteresis phenomena were not observed because the separation flow is divided into a stable conical cavity flow as shown in Figs. 13e–13h. The C_D variation between $L/D < 2.0$ could not be

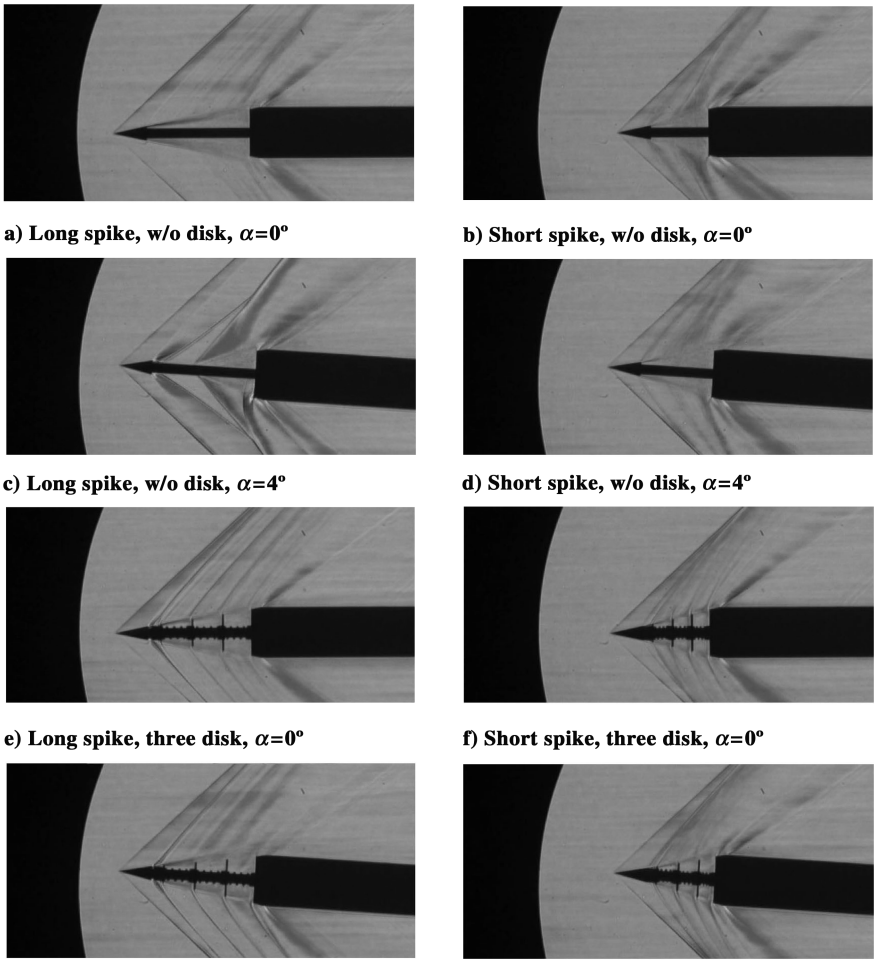

a) Long spike, w/o disk, α=0° **b) Short spike, w/o disk, α=0°**

c) Long spike, w/o disk, α=4° **d) Short spike, w/o disk, α=4°**

e) Long spike, three disk, α=0° **f) Short spike, three disk, α=0°**

g) Long spike, three disk, α=4° **h) Short spike, three disk, α=4°**

Fig. 13 Flow field around telescopic aerospikes at Mach 1.5.

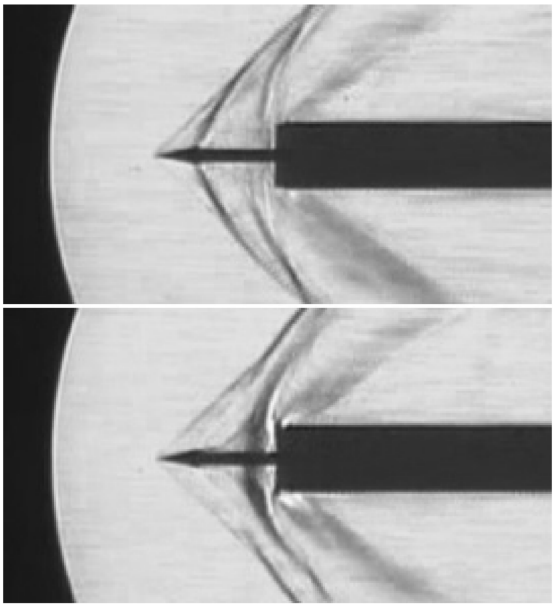

Fig. 14 Dual flow mode of short spike without disk; high and low drag.

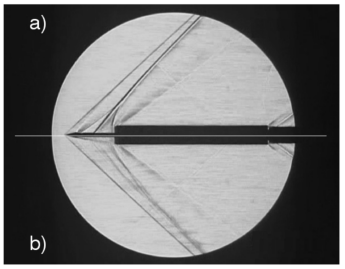

Fig. 15 Flow field around the long spike at Mach 1.5: a) reattachment mode; b) separation mode.

measured for this model because the three outer springs between each disk cancel a part of the inner spring force to retract the spike backward. Table 5 presents a comparison of ΔC_D per unit $\Delta(L/D)$ of the plain aerospike to that of the aerospike with disks at Mach 1.5, 2.0, and 3.0. Negative effects of extending spike were observed for the plain aerospike ($N_d = 0$) at $\alpha = 4$ deg because of the reattachment flow transition, whereas the spike with disks shows better controllability at every Mach number and angle of attack.

Conclusions

Experimental investigations using wind tunnel tests were conducted to show an improved performance of a telescopic aerospike with stabilizer disks. Adding disks to the aerospike is effective for decreasing zero-lift drag and induced drag. Cavities on the conical surface are effective for improving aerodynamic stability. A transition of recirculation/reattachment flow modes of the plain spike causes a large change in C_D. Because of this hysteresis phenomenon, a plain spike is unsuitable for fine aerodynamic control devices. Adding stabilizer disks is effective for improved control of aerospikes.

Table 5 Summary of the C_D controllability of the aerospikes

Aerosipike configuration			$\Delta C_D/\Delta(L/D)$
Mach 1.5	$\alpha = 0$ deg	$N_d = 0$	−0.216
		$N_d = 3$	−0.105
	$\alpha = 4$ deg	$N_d = 0$	+0.107[a]
		$N_d = 3$	−0.039
Mach 2.0	$\alpha = 0$ deg	$N_d = 0$	−0.050
		$N_d = 3$	−0.065
	$\alpha = 4$ deg	$N_d = 0$	+0.258[a]
		$N_d = 3$	−0.039
Mach 3.0	$\alpha = 0$ deg	$N_d = 0$	−0.048
		$N_d = 3$	−0.066
	$\alpha = 4$ deg	$N_d = 0$	−0.000
		$N_d = 3$	−0.040

[a]Reattachment flow mode.

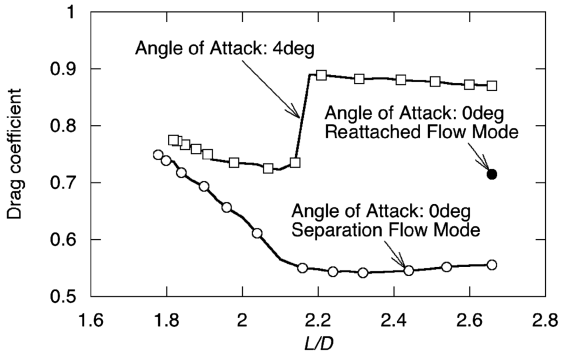

Fig. 16 Variation of drag coefficient with spike L/D, plain spike configuration without disk at Mach 1.5.

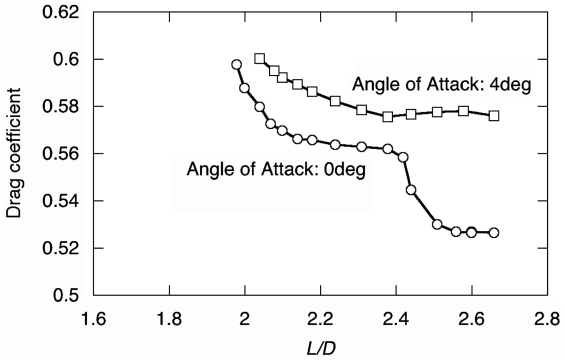

Fig. 17 Variation of drag coefficient with spike L/D, aerospike with three disks configuration at Mach 1.5.

Acknowledgments

This study was supported by the Industrial Technology Research Grant Program in 2004 from the New Energy and Industrial Technology Development Organization (NEDO) of Japan. Y. Maru would like to thank to the Japan Society of the Promotion of Science (JSPS) for their research fellowship. The authors would also like to thank to N. Tanatsugu (Muroran Institute of Technology), M. Hongoh, T. Sato, and T. Kojima (JAXA) for their support.

References

[1] Reding, J. P., Guenther, R. A., and Richter, B. J., "Unsteady Aerodynamic Considerations in the Design of a Drag-Reduction Spike," *Journal of Spacecraft and Rockets*, Vol. 14, No. 1, 1977, pp. 54–60.

[2] Soencksen, K. P., Newill, J. F., and Plostins, P., "Roll Characteristics of the 120-mm M831A1 Projectile," AIAA Paper 2001-0103, 2001.

[3] Soencksen, K. P., Newill, J. F., and Plostins, P., "Aerodynamics of the 120-mm M831A1 Projectile: Analysis of Free-Flight Experimental Data," AIAA Paper 2000-4198, 2000.

[4] Henne, P. A., Howe, D. C., Wolz, R. R., and Hancock, J. L., Jr., "Supersonic Aircraft with Spike for Controlling and Reducing Sonic Boom," US 6,698,684 B1, Mar. 2004.

[5] Robins, A. W., "Preliminary Investigation of the Effects of Several Seeker-Nose Configurations on the Longitudinal Characteristics of a Canard-Type Missile at a Mach Number of 1.60," NACA RM-L53I18, 1953.

[6] Kubota, H., Watanuki, T., Matsumoto, S., Fujita, M., and Fukui, T., "Effect of Spike Attached on a Hemisphere in Hypersonic Flow," *Proceedings of the 19th International Symposium on Space Technology and Science*, edited by Motoki Hinada, The Japan Society for

Aeronautical and Space Science, Tokyo, 1994, pp. 460–467.
[7] Mikhail, A. G., "Spike-Nosed Projectiles: Computations and Dual Flow Modes in Supersonic Flight," *Journal of Spacecraft and Rockets*, Vol. 28, No. 4, 1991, pp. 418–424.
[8] Mikhail, A. G., "Spike-Nosed Projectiles with Vortex Rings: Steady and Nonsteady Flow Simulations," *Journal of Spacecraft and Rockets*, Vol. 33, No. 1, 1996, pp. 8–14.
[9] Feszty, D., Badcock, K. J., and Richards, B. E., "Driving Mechanism of High-Speed Unsteady Spiked Body Flows, Part 1: Pulsation Mode," *AIAA Journal*, Vol. 42, No. 1, 2004, pp. 95–106.
[10] Feszty, D., Badcock, K. J., and Richards, B. E., "Driving Mechanism of High-Speed Unsteady Spiked Body Flows, Part 2: Oscillation Mode," *AIAA Journal*, Vol. 42, No. 1, 2004, pp. 107–113.
[11] Maurer, F., and Brungs, W., "Influencing the Drag and the Bow Wave by Heat Addition in the Stagnation Point of Blunt Bodies in Supersonic Flow," *Proceedings of the 6th Congress of the International Council of the Aeronautical Sciences*, American Institute of Aeronautics and Astronautics, New York, 1968, pp. 174–189.
[12] Srinivasan, G. R., and Chamberlain, R. R., "Drag Reduction of Spiked Missile by Heat Addition," AIAA Paper 2004-4714, 2004.
[13] Menezes, V., Saravanan, S., Jagadeesh, G., and Reddy, K. P. J., "Experimental Investigations of Hypersonic Flow over Highly Blunted Cones with Aerospikes," *AIAA Journal*, Vol. 41, No. 10, 2003, pp. 1955–1966.
[14] Gopalan, J., Menezes, V., Reddy, K. P. J., Hashimoto, T., Sun, M., Saito, T., and Takayama, K., "Flow Fields of a Large-Angle, Spiked Blunt Cone at Hypersonic Mach Numbers," *Transactions of the Japan Society for Aeronautical and Space Sciences*, Vol. 48, No. 160, 2005, pp. 110–116.
[15] Reding, J. P., and Jecmen, D. M., "Effect of External Burning on Spike-Induced Separated Flow," *Journal of Spacecraft and Rockets*, Vol. 20, No. 5, 1983, pp. 452–453.
[16] Shvets, A. L., Gilinsky, M., and Blankson, I. M., "Wind Tunnel Test Results for Gas Flows Inside Axisymmetric Cavities on Cylindrical Bodies with Nose Cones," AIAA Paper 2003-7064, 2003.
[17] Nestler, D. E., "An Experimental Study of Cavity Flow on Sharp and Blunt Cones at Mach 8," AIAA Paper 81-0335, 1981.
[18] Viswanathan, A. K., Squires, K. D., and Forsythe, J. R., "Detached Eddy Simulation of the Flow over an Axisymmetric Cavity," AIAA Paper 2003-265, 2003.
[19] Margason, R. J., and Platzer, M. F., "Effect of Two-Dimensional Cavities on Boundary Layers in Adverse Pressure Gradients," AIAA Paper 97-0300, 1997.
[20] Kobayashi, H., Maru, Y., Hongoh, M., Takeuchi, S., Okai, K., and Kojima, T., "Study on Variable-Shape Supersonic Inlets and Missiles with MRD Device," IAC Paper 05-C4.5.04, 2005.
[21] Kobayashi, H., Kojima, T., Okai, K., and Maru, Y., "Study of Supersonic Cavity Flow in Advanced Variable Geometry Inlet," *Space Technology*, Vol. 25, No. 2, 2005, pp. 63–71.

M. Miller
Associate Editor